Study of resonance in wind parks

Lluis Monjo [a], Luis Sainz [a,*], Jun Liang [b], Joaquín Pedra [a]

[a] Department of Electrical Engineering, ETSEIB-UPC, Av. Diagonal 647, 08028 Barcelona, Spain
[b] School of Engineering, Cardiff University, CF24 3AA Cardiff, UK

A R T I C L E   I N F O

A B S T R A C T

Wind turbine harmonic current emissions are a well-known power quality problem. These emissions flow through wind park impedances, leading to grid voltage distortion. Parallel resonance may worsen the problem because it increases voltage distortion around the resonance frequency. Hence, it is interesting to analyze the parallel resonance phenomenon. The paper explores this phenomenon in wind parks and provides analytical expressions to determine parallel resonances.

1. Introduction

Wind parks (WPs) comprising high power wind turbines (WTs) are increasing in number worldwide [1]. This leads to power quality problems such as WP and main grid current and voltage waveform distortion due to harmonic emissions of WTs equipped with power electronics [1–10]. Several studies have been conducted on these emissions based on actual measurement [1,3–6,8], and probabilistic procedures because WT behavior varies stochastically with time [1–3]. They conclude that dominant WT emissions belong to low-order harmonics (below 1 kHz). Moreover, a high-order harmonic pattern is recognized in the current spectrum between 1.0 and 7.5 kHz due to WT power electronic converter switching frequencies [7]. Recent studies show that WT harmonic emissions are also rich in interharmonics, which are measured and statistically characterized [8,9].

The impact of WT voltage and current emissions on WPs and the main grid can be increased by series and parallel resonances in the collection grid, respectively. Most research works model converters as harmonic current sources and analyze the influence of WP parameters on parallel resonance [1,7,8,11–18]. These studies are mainly based on frequency scan simulations which allow the frequency range and peak impedance values of parallel resonances to be established. Some studies point out analytical expressions to determine the frequency of the first parallel resonance, which can be close to low- and high-order harmonic emissions of WT power electronic converters [13,15]. Studies [7,13] also present a summary of the most important WP harmonic and resonance issues. Recent studies analyze resonance influence on stability of WT power converter control [17,18]. The variables affecting resonances are discussed in most of the previous studies but their influence is not analyzed in depth. In order to investigate this influence further, it is necessary to examine WP resonance frequencies in depth and provide analytical expressions for determining resonance frequencies close to the WT harmonic emission spectrum as a function of WP parameters. Some works also point out that the WT harmonic model as an ideal current source traditionally used to perform frequency scan studies could be inappropriate and provide misleading results because of the possible impact of converter control on resonance [7,17,18]. According to this, WT frequency-dependent models such as Norton equivalent sources are claimed to be used in WP resonance studies. These models would allow considering the influence of WT control on resonance frequencies.

This paper presents analytical expressions to calculate parallel resonance frequencies in onshore WPs and offshore WPs close to shore and thus detect power quality concerns due to WT current emissions. These expressions are obtained from Matlab/Simulink simulations [19] of a generic WP modeling WT behavior as ideal current sources. They are validated by several WP studies where parallel resonances are numerically and analytically identified. These studies also analyze WP parameter influence on resonance.

* Corresponding author. Tel.: +34 93 4011759; fax: +34 93 4017433.
E-mail address: sainz@ee.upc.edu (L. Sainz).

Nomenclature

f_1 fundamental frequency of the grid supply voltage

f, k frequency and harmonic

$f_{p1}, f_{p2}, k_{p1}, k_{p2}$ frequencies and harmonics of the first and second parallel resonances

R_{Tx}, X_{Tx} HV/LV ($x = H$) and MV/LV ($x = L$) transformer impedances

R_L, X_L, X_C MV cable longitudinal and transversal impedances

$R_{L,D}, X_{L,D}, X_{C,D}$ MV cable per-unit length longitudinal and transversal impedances

X_{CB} capacitor bank reactance

η_{N_c}, β_{N_c} coefficients of the second parallel resonance expression

AF_{kpi} amplification factor at the resonance frequency

$Z_{E, kpi}$, $Z_{E, kpi}^{NC}$ impedances with and without capacitors at the resonance frequency

R_{f1}, R_f Resistance values at the fundamental and other frequencies

α_c, α_t MV cable and transformer skin-effect exponents

2. Wind parks

Fig. 1(a) shows a generic WP layout where WTs are supplied through low voltage (LV) underground cables and medium to low voltage (MV/LV) transformers and are interconnected with an $N_r \times N_c$ collection grid of medium voltage (MV) underground cables from the MV collector bus [7,8,11–13,15–17]. Capacitor banks in onshore WPs can also be connected to this bus and harmonic filters are usually installed on the line side of WT converters to mitigate frequency switching harmonics [7,8]. The MV collector bus is connected to the main grid with a high to medium voltage (HV/MV) transformer and a high voltage (HV) overhead line or underground cable in onshore or offshore WPs, respectively.

The harmonic current emissions of WT converters are generally low, and therefore voltage distortion usually remains below standard limits [2,3,10,20,21]. However, the presence of parallel resonance in the WP collection grid may increase voltage distortion above these limits and also affect WP harmonic emissions to the main grid [7,8]. Several works analyze the resonance problem at WT terminals by the frequency scan method and a few points out expressions to calculate the first parallel resonance. In the next Sections, WP harmonic behavior is studied to find analytical expressions for identifying the parallel resonance frequencies closest to the WT harmonic emission spectrum. Although a frequency scan provides more accurate results, it requires high computational effort to simulate different WP configurations with system modeling software and plotting of results obtained [7]. On the other hand, analytical expressions can be a fast, simple and useful engineering tool to analyze resonance frequencies prior to WP design.

3. Wind park harmonic analysis

For harmonic steady-state studies, WPs are modeled by their equivalent circuit (Fig. 1(b)), and the harmonic behavior of the passive set observed from the WTs is studied to identify resonance frequencies. The models of the main grid, HV/MV transformer, MV/LV transformer, MV underground cables and capacitor bank harmonic impedances in Fig. 1(b) (i.e., $\underline{Z}_{S,k}, \underline{Z}_{TH,k}, \underline{Z}_{TL,k}, \underline{Z}_{L,k}, \underline{Z}_{C,k}$ and $\underline{Z}_{CB,k}$, respectively) are as follows [8,12,18]:

$$\underline{Z}_{S,k} = R_S + jk \times X_S = \frac{U_O^2}{S_S} \times \left(\frac{U_{N,M}}{U_{N,H}}\right)^2 \frac{1}{\sqrt{1+\tan^2 \varphi_{Scc}}} (1 + j \times k \times \tan \varphi_{Scc})$$

$$\underline{Z}_{TH,k} = R_{TH} + jk \times X_{TH} = \varepsilon_{THcc} \times \frac{U_{N,M}^2}{S_{THN}} \frac{1}{\sqrt{1+\tan^2 \varphi_{THcc}}} (1 + j \times k \times \tan \varphi_{THcc})$$

$$\underline{Z}_{TL,k} = R_{TL} + jk \times X_{TL} = \varepsilon_{TLcc} \times \frac{U_{N,M}^2}{S_{TLN}} \frac{1}{\sqrt{1+\tan^2 \varphi_{TLcc}}} (1 + j \times k \times \tan \varphi_{TLcc})$$

$$\underline{Z}_{L,k} = R_L + j \times k \times X_L = D \times (R_{L,D} + j \times k \times X_{L,D}) \quad \underline{Z}_{C,k} = -j\frac{X_C}{k} = -j\frac{1}{k} \times \frac{1}{D} \times 2 \times X_{C,D}$$

$$\underline{Z}_{CBk} = -j\frac{X_{CB}}{k} = -j\frac{1}{k} \times \frac{U_{N,M}^2}{Q_C},$$

$$\text{(1)}$$

where $k = f_k/f_1$ (with f_k and f_1 being the harmonic and fundamental frequencies, respectively) and, according to Fig. 1(a), U_O, S_S and $\tan \varphi_{Scc}$ are the main grid open-circuit voltage, short-circuit power and X_S/R_S ratio at the point of coupling.

- $U_{N,H}/U_{N,M}$, S_{THN}, ε_{THcc} and $\tan \varphi_{THcc}$ are the HV/MV transformer rated voltages and power, per-unit short-circuit impedance and X_{TH}/R_{TH} ratio.
- $U_{N,M}/U_{N,L}$, S_{TLN}, ε_{TLcc} and $\tan \varphi_{TLcc}$ are the MV/LV transformer rated voltages and power, per-unit short-circuit impedance and X_{TL}/R_{TL} ratio.
- $R_{L,D}$, $X_{L,D}$ and $X_{C,D}$ are the MV cable per-unit-length longitudinal and parallel impedances and D is the MV cable length.
- Q_C is the capacitor bank reactive power consumption (i.e., the capacitor bank size).

Note that the following assumptions are made to develop the study from Fig. 1(b):

- Although, in order to consider the influence of WT control on consumed harmonic currents, WTs are better characterized as Norton equivalent sources [7], the typical WT harmonic model as ideal current source is used in the study because it is commonly chosen to perform frequency scan studies and it offers a useful insight into parallel resonance analysis [1,8,11–14,16]. However, further research is required to analyze the impact of WT control on this resonance.
- A distributed parameter model of the cables could be required for more accurate WP resonance analysis [7,16,17], but a concentrated parameter model is assumed because it provides good insights into the resonance problem and is commonly used in WP resonance studies [1,7,8,13,15].
- Only onshore WPs and offshore WPs close to shore (i.e., connected to the main grid through a short length underground cable of a few kilometers [1]) are considered in the study because the transversal impedance of the HV overhead line and underground cable is not considered (the longitudinal impedance is included in the impedances of the main grid and HV/MV transformer).
- LV underground cables are omitted because they are short, and therefore the capacitance values are very small and their longitudinal impedance can be included in the impedance of the MV/LV transformer.
- WT harmonic filters are not considered because they are only rated about 50 kvar per WT, and therefore only aggregation of filters for many WTs would shift the natural resonance of the WP [7]. Nevertheless, their possible influence on resonance frequencies is discussed in Section 6.3.

Frequency scan analysis makes it possible to numerically determine resonances observed from any wind turbine [7]. As an example, Fig. 2(a) shows, labeled as Simulation no. 1, the frequency response of the system equivalent impedance without capacitor banks (i.e., $Q_C = 0$, and therefore $X_{CB} = \infty$) at bus
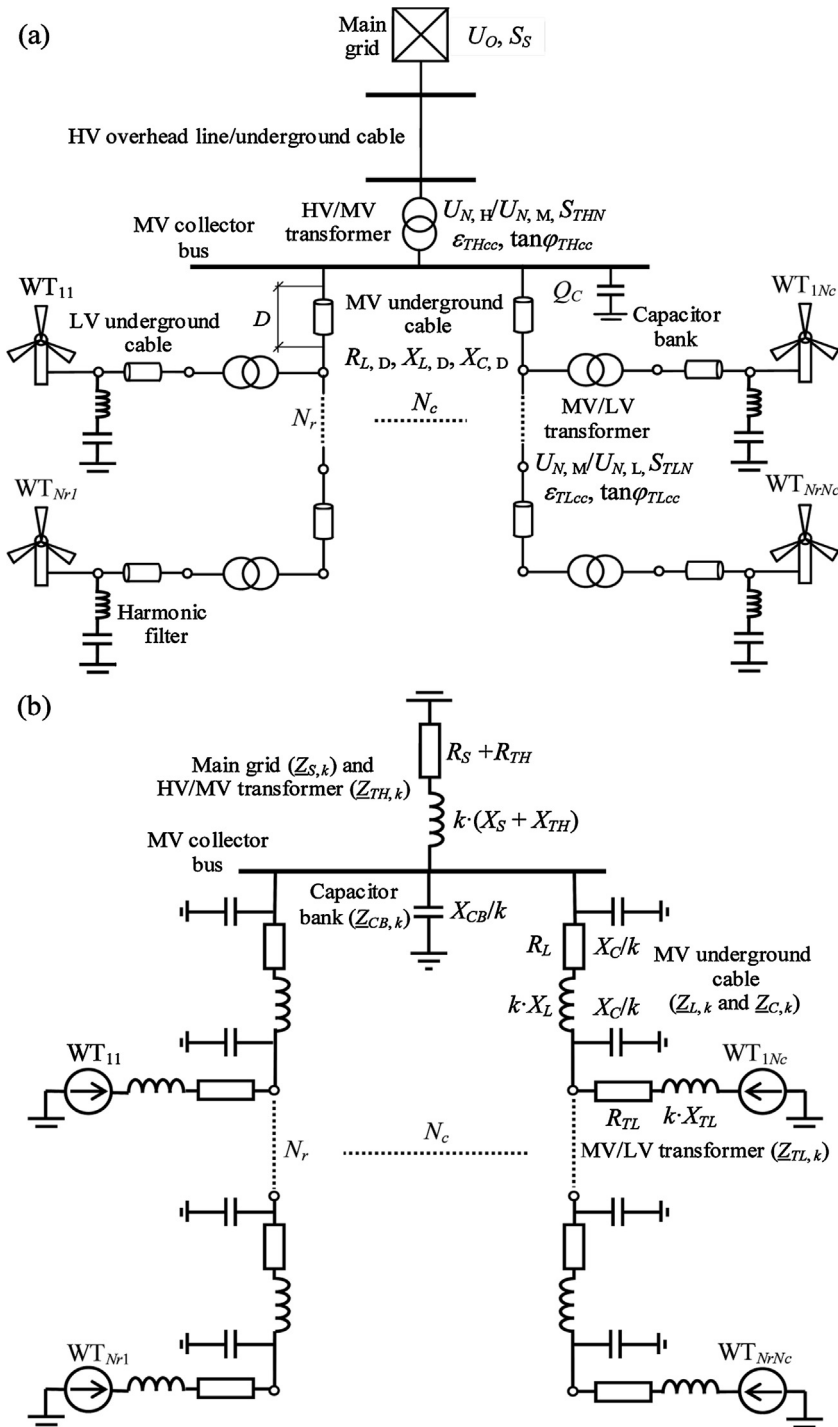
Fig. 1. Wind park: (a) Typical wind park layout. (b) Wind park equivalent circuit.

N_r1 (i.e., from WT$_{Nr1}$) for four different WP layouts. This response was numerically obtained by Matlab/Simulink simulations [19] considering the WP parameters in Table 1 (data no. 1 [6]) and is referred to the MV level. Fig. 2(a) illustrates that two parallel resonances, $k_{p1} \approx 28, 34, 49, 56, 72$ and 106 (i.e., $f_{p1} = k_{p1} \cdot f_1 = k_{p1} \cdot 50 \approx 1.4, 1.7, 2.45, 2.8, 3.6$ and 5.3 kHz) and $k_{p2} \approx 110$ and 165 (i.e., $f_{p2} = k_{p2} \cdot f_1 = k_{p2} \cdot 50 \approx 5.5$ and 8.25 kHz), can appear close to harmonic emission frequencies of WT converters, and should therefore be analyzed to prevent harmonic power quality problems [7–9,13]. It must be noted that these resonances depend not only on WP electrical parameters, but also on WP

configuration (i.e., number of rows N_r and columns N_c of the WP collection grid in Fig. 1(a)). Two additional frequency scan simulations are also shown in Fig. 2(a) in order to check the assumptions about WP resistances and MV/LV transformers in the study,

- Simulation no. 2: System frequency response with WP resistances fifty times higher is shown in gray lines to illustrate that they damp system harmonic response but do not affect resonance frequency identification significantly; hence, they can be neglected [8]. This damping phenomenon, which is discussed in Section 6.2, is mainly produced by the frequency-dependent resistance of WP cables and transformers due to the skin effect [7,8,17].
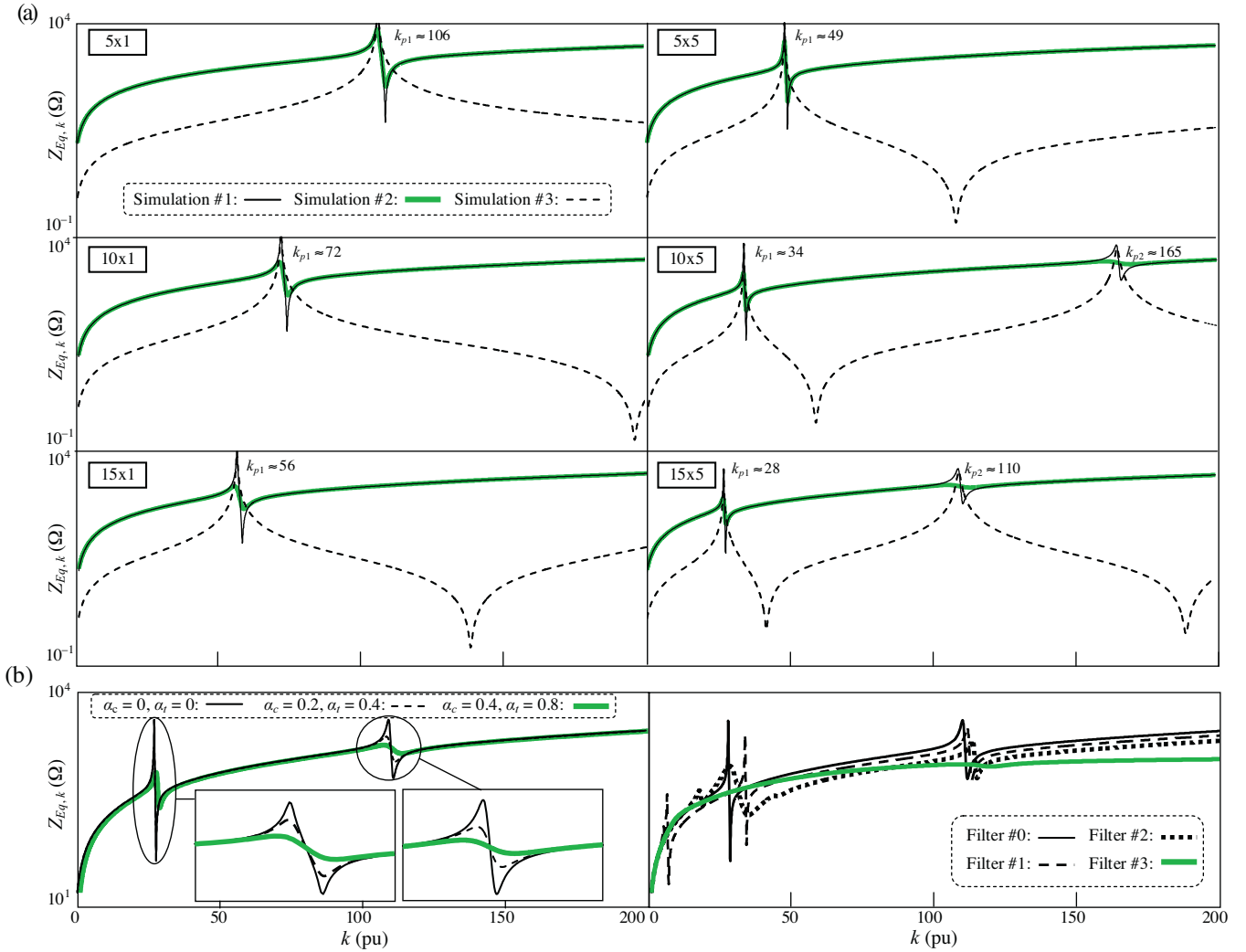
Fig. 2. Wind park harmonic response: (a) frequency scan simulations. (b) Influence of the skin effect (left) and the wind turbine harmonic filters (right).

- Simulation no. 3: System frequency response without MV/LV transformers is shown in dashed black lines to illustrate that these transformers can be omitted in the study of parallel resonance observed from WTs because they do not affect parallel resonance frequency significantly. On the other hand, they influence series resonance and the equivalent impedance values of frequencies beyond the parallel resonance point.

Table 1
Wind park parameters.

	Parameters	Data no. 1 [6]	Data no. 2
Main grid	U_0	110 kV	110 kV
	S_S	4200 MV A	25000 MV A
	$\tan \varphi_{Scc}$	18 pu	18 pu
HV/MV transformer	$U_{N,H}/U_{N,M}$	110/30 kV	110/30 kV
	S_{THN}	250 MV A	125 MV A
	ε_{THcc}	12%	5%
	$\tan \varphi_{THcc}$	12 pu	10 pu
MV/LV transformer	$U_{N,M}/U_{N,L}$	30/0.69 kV	30/0.69 kV
	S_{TLN}	3 MV A	5 MV A
	ε_{TLcc}	5%	5%
	$\tan \varphi_{TLcc}$	12 pu	10 pu
MV underground cable	$R_{L,D}$	0.13 Ω/km	0.13 Ω/km
	$X_{L,D}$	0.112 Ω/km	0.112 Ω/km
	$X_{C,D}$	12.73 kΩ km	12.73 kΩ km
	D	0.32 km	0.5 km
Capacitor bank	Q_C	0 … 50 MVar	0 MVar

4. Harmonic resonance without capacitor banks

As pointed out in the previous Section, the harmonic of the parallel resonances observed from any WT mainly depends on the WP reactances (resistances are neglected) and rows N_r and columns N_c of the collection grid. To study the identification of the first and second parallel resonances, Matlab/Simulink extensive simulations were made by varying the WP rows and columns from 1 to 20 (i.e., N_r = 1 to 20 and N_c = 1 to 20) and considering data no. 1 in Table 1 without capacitor banks (i.e., Q_C = 0, and therefore $X_{CB} = \infty$).

The harmonics of the parallel resonances observed from bus N_r1 for all the row and column combinations were numerically identified by simulation. Fig. 3(a) shows harmonics k_{p1} and k_{p2} of the first and second parallel resonances as a function of the collection grid rows N_r and for different values of the collection grid columns N_c. The harmonics of the parallel resonances in Fig. 2(a) are labeled with black dots in Fig. 3(a). From these results, it must be noted that

- Harmonic k_{p1} of the first parallel resonance depends on the WP electrical parameters and the $N_r \times N_c$ layout. The expression to determine k_{p1} can be deduced by considering that $k_{p1} \cdot X_L$ is much lower than $k_{p1} \cdot (X_S + X_{TH})$ and X_C/k_{p1}. From this assumption, the equivalent circuit without capacitor banks in Fig. 1(b) can be simplified to the circuit in Fig. 4(a) with $X_{CB} = \infty$, and the expression
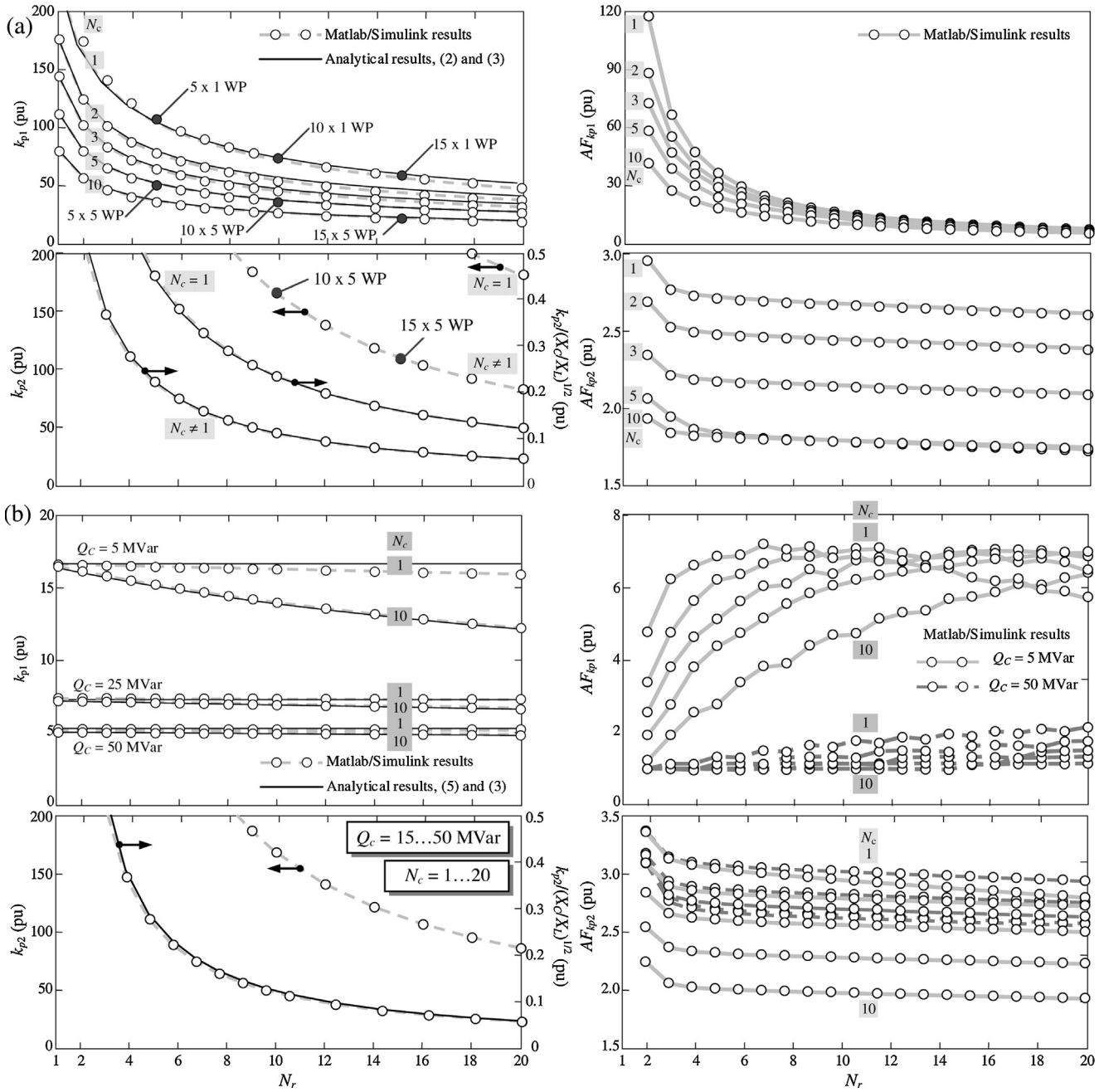
Fig. 3. Wind park parallel resonance (data no. 1 in Table 1): (a) Parallel resonance without capacitor banks. (b) Parallel resonance with capacitor banks.

of the harmonic of the first parallel resonance observed from any WT is

$$k_{p1} \times (X_S + X_{TH}) = \frac{X_C}{2} \frac{1}{N_r \times N_c} \frac{1}{k_{p1}} \Rightarrow k_{p1} = \frac{1}{\sqrt{2}} \times (N_r \times N_c)^{-0.5}$$

$$\times \sqrt{\frac{X_C}{X_S + X_{TH}}}. \quad (2)$$

To validate (2), the harmonic k_{p1} calculated with the above expression and data no. 1 in Table 1 is compared with the simulation results in Fig. 3(a). It is numerically verified that the error with respect to the frequency scan results is below 10%.

• Harmonic k_{p2} of the second parallel resonance depends on the WP electrical parameters and the $N_r \times N_c$ layout. However, this resonance is independent of the collection grid columns for $N_c \neq 1$. The expression to determine k_{p2} is deduced by considering that

$k_{p2} \cdot (X_S + X_{TH})$ is much higher than $k_{p2} \cdot X_L$ and X_C/k_{p2}. From this assumption, the equivalent circuit without capacitor banks in Fig. 1(b) can be simplified to the circuit in Fig. 4(b) and the expression of k_{p2} is a function of the MV underground cable ratio X_C/X_L and the collection grid layout. This expression could be deduced from the study of the equivalent circuit in Fig. 4(b) but it is no easy task. For this reason, it is determined with an empirical formula which is a function of the MV underground cable ratio X_C/X_L and the number of rows N_r and columns N_c of the collection grid. To deduce this formula, k_{p2} in Fig. 3(a) is divided by the ratio $(X_C/X_L)^{1/2}$, and the obtained curves in Fig. 3(a) are fitted with a power function of N_r:

$$k_{p2} = \eta_{N_c} \times N_r^{-\beta_{N_c}} \times \sqrt{\frac{X_C}{X_L}} \qquad \begin{array}{ll} \eta_{N_c=1} = 1.979, & \beta_{N_c=1} = 0.929 \\ \eta_{N_c \neq 1} = 1.087, & \beta_{N_c \neq 1} = 0.992 \end{array}.$$
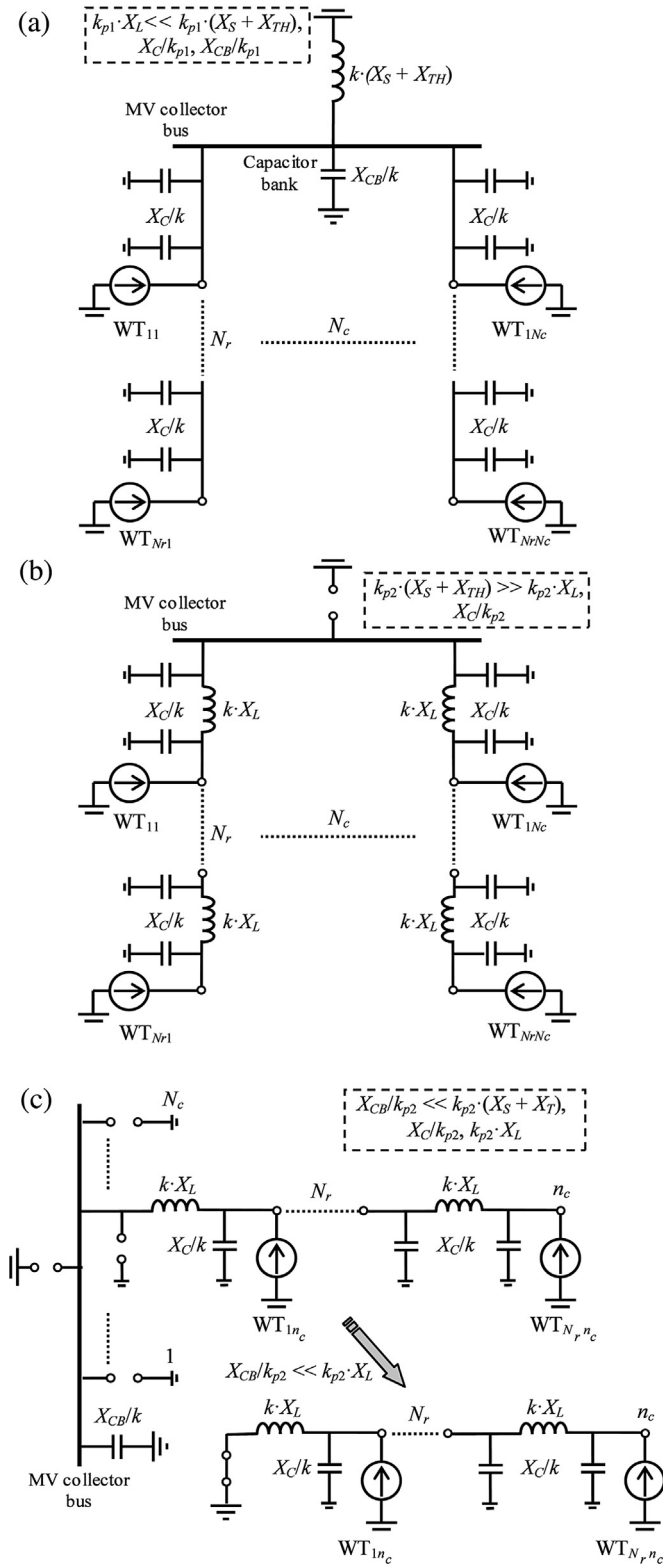
$$(3)$$

Fig. 4. Wind park equivalent circuits: (a) Equivalent circuit at harmonic k_p with and without capacitor banks. (b) Equivalent circuit at harmonic k_p without capacitor banks. (c) Equivalent circuit at harmonic k_p with capacitor banks.

To validate (3), the harmonic k_{p2} calculated with this expression and data no. 1 in Table 1 is compared with the simulation results in Fig. 3(a). It is verified that the error with respect to the frequency scan results is below 5%. Moreover, the influence of WP parameters on the accuracy of (3) is verified by 10,000-shot Monte Carlo

simulations according to uniform distributions based on the WP data in Table 1.

In addition to frequency, parallel resonance is also characterized by its impedance amplification factor, which determines the severity of the consequences of resonance. For this reason, the amplification factors of parallel resonances observed from bus N_r1 for all row and column combinations are numerically determined by simulation. These factors are defined as the ratio between the value of the harmonic impedance with and without WP capacitors ($Z_{E,kpi}$ and $Z_{E,kpi}^{NC}$, respectively) at the resonance frequency $f_{pi} = k_{pi} \cdot f_1$ ($i = 1, 2$), i.e.,

$$\mathrm{AF}_{kpi} = \frac{Z_{E,kpi}}{Z_{E,kpi}^{NC}} \qquad (i = 1, 2). \tag{4}$$

According to (4) and the Matlab/Simulink simulations, Fig. 3(a) shows the impedance amplification factors of the first and second parallel resonances (i.e., $\mathrm{AF}_{k_{p1}}$ and $\mathrm{AF}_{k_{p2}}$) observed from bus N_r1 as a function of the collection grid rows N_r and for different values of the collection grid columns N_c. It can be observed that larger WPs lead to smaller amplification factors.

5. Harmonic resonance with capacitor banks

The connection of capacitor banks to the MV collection bus affects parallel resonances. To study the identification of these resonance frequencies, extensive Matlab/Simulink simulations were made varying the WP rows N_r and columns N_c from 1 to 20 for ten steps of the capacitor bank size Q_C (i.e., $0.1 \cdot Q_C$ to Q_C) and considering data no. 1 in Table 1. The first and second harmonics of the parallel resonances observed from bus N_r1 for all the row and column combinations were numerically identified by simulations. Fig. 3(b) shows harmonic k_{p1} of the first parallel resonance as a function of the collection grid rows N_r and for two different values of the collection grid columns N_c and three capacitor bank sizes. Fig. 3(b) shows harmonic k_{p2} of the second parallel resonance as a function of the collection grid rows N_r and for any number of WP columns and capacitor bank size (resonances are approximately independent of both variables). From these results, it must be noted that

- Harmonic k_{p1} of the first parallel resonance depends on the WP electrical parameters, the capacitor bank reactance and the $N_r \times N_c$ layout, with the capacitor bank reactance being the most influential variable. The expression to determine k_{p1} can be deduced by considering that $k_{p1} \cdot X_L$ is much lower than $k_{p1} \cdot (X_S + X_{TH})$, X_C/k_{p1} and X_{CB}/k_{p1}. From this assumption, the equivalent circuit with capacitor banks in Fig. 1(b) can be simplified to the circuit in Fig. 4(a), and the expression of the harmonic of the first resonance observed from any WT is

$$k_{p1} \times (X_S + X_{TH}) = \frac{X_{CEq}}{k_{p1}} \Rightarrow k_{p1} = \sqrt{\frac{X_{CEq}}{X_S + X_{TH}}}$$

$$X_{CEq} = \frac{X_{CB} \times \left(X_C/2\right) \left(1/(N_r \times N_c)\right)}{X_{CB} + \left(X_C/2\right) \left(1/(N_r \times N_c)\right)}. \tag{5}$$

To validate (5), the harmonic k_{p1} calculated with this expression and data no. 1 in Table 1 is compared with the simulation results in Fig. 3(b). It is verified that the error with respect to the simulations of the frequency scan results is below 2%.

- Harmonic k_{p2} of the second parallel resonance only depends on the WP electrical parameters and the collection grid rows N_r. Beyond this, it can be observed that this resonance in Fig. 3(b) is produced at the same harmonic values as the second parallel resonance without capacitor banks and $N_c \neq 1$ in Fig. 3(a).

Thereby, harmonic k_{p2} can be determined by the empirical formula in (3) with $N_c \neq 1$. To validate this, the harmonic k_{p2} calculated with this expression and data no. 1 in Table 1 is compared with the simulation results in Fig. 3(b). It is numerically verified that the error with respect to the frequency scan results is below 6.5%. The expression of k_{p2} can be analyzed by consider that X_{CB}/k_{p2} is much lower than $k_{p2} \cdot (X_S + X_{TH})$ and X_C/k_{p2}. From this assumption, the equivalent circuit with capacitor banks in Fig. 1(b) can be simplified to the circuit in Fig. 4(c), and the expressions of k_{p2} only depend on the MV underground cable ratio X_C/X_L and the collection grid rows N_r. Actually, the circuit in Fig. 4(c) is the same as that derived from Fig. 4(b) for case $N_c \neq 1$.

In addition to the resonance frequencies and according to (4) and the Matlab/Simulink simulations, Fig. 3(b) shows the impedance amplification factor of the first and second parallel resonances (i.e., $AF_{k_{p1}}$ and $AF_{k_{p2}}$) observed from bus N_r1 as a function of the collection grid rows N_r and for different values of the collection grid columns N_c and capacitor bank sizes Q_C. It can be observed that larger WPs lead to smaller amplification factors. This is also true for capacitor bank size.

6. Impact of WP characteristics on resonance

The studies in Sections 4 and 5 are performed for symmetrical $N_r \times N_c$ WPs (i.e., WPs with the same number of WTs, N_r, for each of their N_c columns) and considering neither WP resistances nor MV/LV transformers. In the following subsections, the influence of these assumptions is analyzed.

6.1. Deviations from the WP row and column symmetry

It is checked by simulations that, according to Fig. 4(a), the expressions of the first parallel resonance in (2) and (5) can be generalized for any deviation from WP symmetry (i.e., for any number of WTs of each column), as follows:

$$k_{p1} = \sqrt{\frac{X_{CEq}}{X_S + X_{TH}}}, \quad X_{CEq} = \frac{X_{CB} \times \sum_{n=1}^{N_c} X_{C,n}}{X_{CB} + \sum_{n=1}^{N_c} X_{C,n}}, \quad X_{C,n} = \frac{X_C}{2} \frac{1}{N_{r,n}},$$

(6)

where $X_{C,n}$ is the equivalent capacitor of the nth column ($n = 1$ to N_c) and $N_{r,n}$ is the number of WTs (or rows) of each one of the nth columns. It can be observed that (2) and (5) can be derived from (6) if $N_{r,n} = N_r$ ($n = 1$ to N_c) and that no capacitor bank is connected (i.e., $Q_C = 0$, and therefore $X_{CB} = \infty$) and if $N_{r,n} = N_r$ ($n = 1$ to N_c), respectively. It is also numerically verified that the expressions of the second parallel resonance in (3) cannot be generalized for any deviation from WP symmetry because it mainly depends on MV cable parameters (see Fig. 4(b)). Thus, it is difficult to obtain a general analytical expression of this resonance for any WP configuration.

6.2. Frequency-dependent resistances

According to Fig. 2(a), WP resistances damp system harmonic response but do not affect resonance frequency. The damping phenomenon, mainly produced by the frequency-dependent resistance of WP cables and transformers due to the skin effect, is analyzed in this Section. This effect is modeled as in [8]:

$$R_f = R_{f_1} \times \left(\frac{f}{f_1}\right)^{\alpha_d} \quad (d = c, t),$$

(7)

where R_{f_1} and R_f are the resistances at the fundamental frequency f_1 and the analyzed frequency f, respectively, and α_d with $d = c$ and t

are the cable and transformer skin-effect exponents, which usually range from 0 to 0.4 and 0 to 0.8, respectively.

Fig. 2(b) shows the influence of the skin effect on the frequency response of the 15×5 system equivalent impedance in Fig. 3. These results are obtained by considering (7) in the resistances of the WP underground cables and transformers (1). It is observed that the frequency-dependent resistance has no impact on the resonance frequencies but damps the equivalent impedance at these frequencies (the impedance at frequencies beyond the resonance point is not much affected). Obviously, the damping phenomenon becomes more pronounced with increasing the resonance frequency [7,8,17].

6.3. Passive harmonic filters

Shunt filters are installed at WT buses (between WTs and MV/LV transformers) for harmonic mitigation of large WTs [7,8]. In order to determine the possible influence of these filters on the frequency response of the WP equivalent impedance, three examples with different filters connected at all WT buses were performed in the 15×5 system in Fig. 3:

- Filter no. 1: Notch filters tuned at the 7th harmonic order.
- Filter no. 2: Notch filters tuned at the 25th harmonic order.
- Filter no. 3: Second-order high-pass filters tuned at the 13th harmonic order.

Fig. 2(b) shows the results (the 15×5 system without filters is labeled as Filter no. 0). Notch filters produce a valley around the tuned frequency which can shift and damp the natural parallel resonance of WPs if this frequency is close enough to the parallel resonance point of the unfiltered system. However, a significant equivalent impedance peak still appears because of the filter and WP impedances. Second-order high-pass filters damp resonance above the tuned frequency and they seem more effective than notch filters. Note that the study was performed for specific cases, and therefore further research is required to fully understand WT filter influence on WP resonance.

7. Application of harmonic resonance identification

The parallel resonances of a 4×6 WP with data no. 2 in Table 1 (called Case no. 1) are numerically and analytically obtained from Matlab/Simulink simulations and the expressions in the paper, respectively. The cable and transformer skin effect (7) is also considered in the simulations with skin factors $\alpha_c = 0.2$ and $\alpha_c = 0.4$, respectively. The resonances of the following four cases are studied to illustrate the influence of the main grid short-circuit power, MV cable length, WP size and capacitor bank connection:

- Case no. 2: A weak grid with $S_S = 2500$ MV A (i.e., with $S_S/S_N = 20$) is considered.
- Case no. 3: WTs are up to 1 km away from each other.
- Case no. 4: WP size is reduced to a 2×2 layout.
- Case no. 5: A capacitor bank of 40 MV A is connected.

Fig. 5 plots the frequency response of all cases studied and Table 2 shows the numerical (N) and analytical (A) results of the parallel resonances. The accuracy of the analytical expressions with a maximum error of 2% is worth noting. The following conclusions can be drawn:

- Case no. 2: Weak grids with low short-circuit power can shift the first resonance to the 1.0 to 2.0 kHz frequency range of the WT
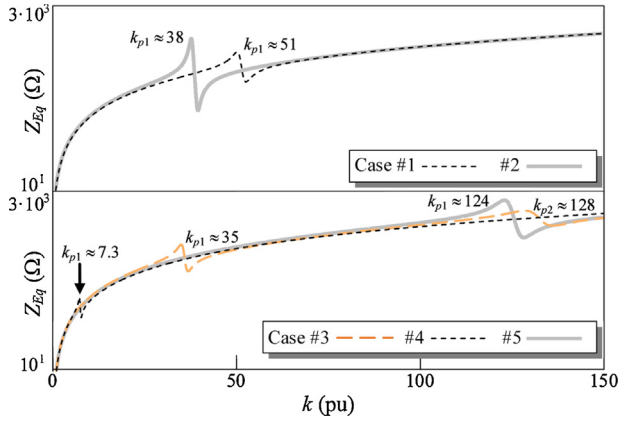
Fig. 5. Wind park harmonic response.

high-order harmonic emission pattern due to the large values of the grid reactance X_S (see $Z_{S,k}$ expression in (1)) and lead to low k_{p1} resonance values in (2), (5) and (6). According to (3), the second resonance is not affected by the main grid short-circuit power.

- Case no. 3: WTs far away from each other can also shift resonances to the 1.0 to 2.0 kHz frequency range of the WT high-order harmonic emission pattern in WPs without capacitor banks because the first parallel resonance (2) is inversely proportional to the square root of the cable length and the second parallel resonance (3) is inversely proportional to the cable length:

$$k_{p1} = (N_r \times N_c)^{-0.5} \sqrt{\frac{1}{D}} \times \sqrt{\frac{X_{C,D}}{X_S + X_{TH}}}$$

$$k_{p2} = \frac{1}{\sqrt{2} \times D} \times \eta_{N_c} \times N_r^{-\alpha_i} \times \sqrt{\frac{X_{C,D}}{X_{L,D}}}. \quad (7)$$

The previous comments can be verified in the examples where, considering the resonance frequencies of case no. 1, the resonance frequencies of case no. 3 can be approximately calculated as $51 \cdot (0.5/1)^{1/2} = 36.1$ and $260 \cdot (0.5/1) = 130$.

- Case no. 4: From the analytical expressions of the parallel resonances, it can be observed that these resonances are closer to low-order harmonics in large WPs than in small WPs because parallel resonance frequencies move to lower order harmonics when the columns and rows of WPs increase.
- Case no. 5: In WPs with capacitor banks, these banks modify parallel resonances but only the first is directly affected (the larger the capacitor size, the lower the harmonic order of the first parallel resonance). This resonance mainly depends on the main grid and HV/MV transformer reactance and the capacitor bank size (5). Thus, in these WPs, only parallel resonance k_{p2} is affected by cable length and is inversely proportional to this length, as in WPs without capacitor banks (7).

Note that the expressions in the paper are useful to determine that, in the studied cases, the frequency of resonance k_{p2} is greater than WT harmonic emissions.

The voltage distortions $HD_{vk} = V_k/V_1$ at bus N_r1 (i.e., at WT$_{Nr1}$ terminals where the resonance is analyzed) and at the collector bus are numerically obtained from Matlab/Simulink simulations considering the following WT harmonic emissions (magnitude and phase angle): (i) The harmonic current limits in the German Electricity Association (VDEW) Standard for generators connected to medium voltage networks are set as the WT emission magnitudes I_k (or $HD_{ik} = I_k/I_1$) [10]. This standard provides specific
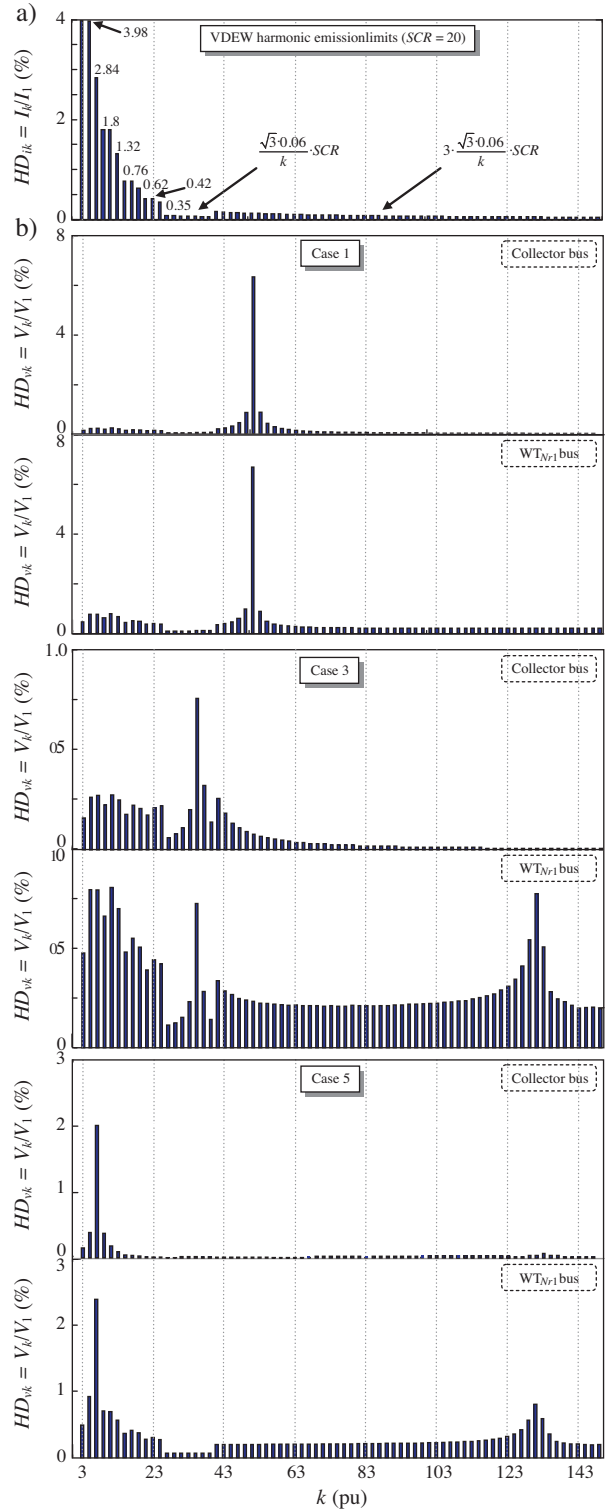

Fig. 6. Wind park harmonic distortions: (a) VDEW current emission limits. (b) Voltage distortions.

magnitude values of the generator (or WT) harmonic limits based on the grid short-circuit ratio *SCR* which can be easily included in the simulation program. The limits for a short-circuit ratio of 20 (i.e., for a pu grid impedance of 5%) are quite similar (in particular, harmonics below 1.5 kHz) to the distortion limits in IEEE Standard 15471 [21]. (ii) Regarding harmonic current phase angles, no data

Table 2
Application results (N: numerical. A: analytical).

$k_{pi}^{(Num)}$ and $k_{pi}^{(An)}$	Case									
	No. 1		No. 2		No. 3		No. 4		No. 5	
	N	A	N	A	N	A	N	A	N	A
1	51	52	38	38	35	36	124	127	7.3	7.5
2	260	262	260	263	128	131	515	521	260	262

are available but it is commonly accepted that they are uniformly distributed over the [0, 2·π] interval (in particular, high-order harmonics) [2,3]. Thus, harmonic voltage distortions are obtained from the 95% percentile value of 10,000-shot Monte Carlo Matlab simulations where the harmonic current phase magnitudes are set according to the VDEW Standard and the harmonic current phase angles of each WT are randomly set according to the distribution $U(0, 2\pi)$. Fig. 6(a) plots the VDEW current emission limits used in the simulations and Fig. 6(b) plots the voltage distortions for Cases nos. 1, 3 and 5. The voltage distortion pattern obtained at both buses around the first resonance frequency is similar and the frequency of the maximum distortion values matches with the parallel resonance frequency. Nevertheless, distortions at the collector bus are much lower than those at bus N_r1 for the second parallel resonance because this resonance does not occur at the collector bus. The comparison of Cases no. 1 and no. 3 shows that higher and more dangerous harmonic voltage distortions can occur when the parallel resonance ($k_{p1} = 51$) matches exactly with some frequencies of the WT harmonic emissions than when it is close ($k_{p1} = 7.3$) to them. It must be noted that the performed study is just an example, and therefore further research is required to accurately evaluate the impact of resonance on WP power quality. WP data (e.g., magnitudes and phase angles of WT harmonic emissions or cable and transformer skin-effect exponents) can affect voltage distortions significantly.

8. Conclusions

This paper presents analytical expressions to determine parallel resonance frequencies in onshore WPs and offshore WPs close to shore with and without capacitor banks. These expressions are useful to detect power quality problems due to WT harmonic current emissions and to analyze the influence of grid short-circuit power and WP parameters on resonance. The analytical expressions are validated by analyzing the frequency response of several WP simulations. Offshore WPs far from shore could be investigated to study the influence of long-length HV underground cables on parallel resonance based on the proposed resonance study framework. Moreover, other WP layouts could be examined to determine the effect of WT distribution on resonance.

Acknowledgment

References

[1] L.H. Kocewiak, Harmonics in Large Offshore Wind Farms (Thesis for the PhD Degree in Electrical Engineering), Dep. of Energy Technology, Aalborg University, Denmark, 2012, April http://vbn.aau.dk/files/62660098/lukasz_kocewiak.pdf

[2] S.A. Papathanassiou, M.P. Papadopoulos, Harmonic analysis in a power system with wind generation, IEEE Trans. Power Delivery 21 (Oct (4)) (2006) 2006–2016.

[3] S.T. Tentzerakis, S.A. Papathanassiou, An investigation of the harmonic emissions of wind turbines, IEEE Trans. Energy Convers. 22 (March (1)) (2007) 150–158.

[4] D. Schulz, R.E. Hanitsch, Investigation of the current harmonic parameters of wind energy converters, in: Proceedings of the IEEE Power Tech. Conference (2003), June, Bologna, Italy. vol. 3, 2003.

[5] T. Thiringer, T. Petru, C. Liljegren, Power quality impact of a sea located hybrid wind park, IEEE Trans. Energy Convers. 16 (Jun (2)) (2001) 123–127.

[6] J.I. Herrera, T.W. Reddoch, J.S. Lawler, Harmonics generated by two variable speed wind generating systems, IEEE Trans. Energy Convers. 3 (Jun (2)) (1988) 267–273.

[7] IEEE, PES Wind Plant Collector System Design Working Group, Harmonics and resonances issues in wind power plants, in: Proceedings of the IEEE Power and Energy Society General Meeting, 2012, pp. 1–8.

[8] K. Yang, On Harmonic Emissions, Propagation and Aggregation a Wind power Plants (Doctoral Thesis), Dep. of Engineering Sciences and Mathematics, Lulea University of Technology, Sweden, 2015, March http://pure.ltu.se/portal/en/

[9] K. Yang, M. Bollen, M. Wahlberg, Measurement at two different nodes of a wind-park, in: Proceedings of the IEEE Power and Energy Society General Meeting, 2012, pp. 1–7.

[10] A.A. Rockhill, M. Liserre, R. Teodorescu, P. Rodríguez, Grid-filter design for a multimegawatt medium-voltage source inverter, IEEE Trans. Ind. Electron. 58 (4) (2013) 1205–1216.

[11] U. Axelsson, U. Holm, M. Bollen, K. Yang, Propagation of harmonic emission from the turbines through the collection grid to the public grid, in: Proceedings of the 22nd International Conference and Exhibition on Electricity Distribution (CIRED 2013), June, Stockholm, Sweden, 2013, pp. 1–4.

[12] R. Zheng, M. Bollen, J. Zhong, Harmonic resonances due to a grid-connected wind farm, in: Proceedings of the 14th International Conference on Harmonics and Quality of Power (ICHQP 2010), September, Bergamo, Italy, 2010, pp. 1–7.

[13] J. Li, N. Samaan, S. Williams, Modeling of large wind farm systems for dynamic and harmonics analysis, in: Proceedings of the IEEE/PES Transmission and Distribution Conference and Exposition, April, 2008, pp. 1–7.

[14] J. Balcells, D. Gonzalez, Harmonics due to resonance in a wind power plant, in: Proceedings of the 8th IEEE Int. Conf. on Harmonics and Quality of Power (ICHQP 1998), Nov, Athens, Greece, 1998, pp. 896–899.

[15] S. Schostan, K.-D. Dettmann, D. Schultz, J. Plotkin, Investigation of an atypical sixth harmonic current level of a 5 MW wind turbine configuration, in: Proceedings of the Int. Conf. on Computer as a Tool (EUROCON), September, 1998.

[16] F. Ghassemi, K.-L. Koo, Equivalent network for wind farm harmonic assessments, IEEE Trans. Power Delivery 25 (July (3)) (2010) 1808–1815.

[17] S. Zhang, S. Jiang, X. Lu, B. Ge, F. Zheng, Resonance issue and damping techniques for grid-connected inverters with long transmission cable, IEEE Trans. Power Electron. 29 (1) (2014) 110–120.

[18] X. Wang, F. Blaabjerg, W. Wu, Modeling and analysis of harmonic stability in an AC power-electronics-based power system, IEEE Trans. Power Electron. 29 (12) (2014) 6421–6432.

[19] Matlab 7.9, (R2009b) and Simulink, The MathWorks, Natick, MA, 2009.

[20] E.N. Standards, Voltage Characteristics of Electricity Supplied by Public Electricity Networks, vol. 3, EN 50160 Ed., 2003.

[21] IEEE, Standard for interconnecting distributed resources with electric power systems, in: IEEE Standard 15471, 2005.